VIII International Conference on Fracture Mechanics of Concrete and Concrete Structures
FraMCoS-8
J.G.M. Van Mier, G. Ruiz, C. Andrade, R.C. Yu and X.X. Zhang (Eds)

EVALUATION OF THE TENSILE STRENGTH OF SFRC AS DERIVED FROM INVERSE ANALYSIS OF NOTCHED BENDING TESTS

ALI AMIN[*], STEPHEN J. FOSTER[*], AND AURELIO MUTTONI[†]

[*] The University of New South Wales, School of Civil and Environmental Engineering
Centre for Infrastructure Engineering and Safety, Sydney, Australia
e-mail: ali.amin@unsw.edu.au - Web page: http://www.unsw.edu.au/

[†] École Polytechnique Fédérale de Lausanne,
School Architecture, Civil and Environmental Engineering, Lausanne, Switzerland
email: aurelio.muttoni@epfl.ch - Web page: http://www.epfl.ch/

Key words: Steel fibre, concrete, inverse analysis, bending, uniaxial tension, prism tests.

Abstract: For the design of SFRC members, the most fundamental material property is its post cracking residual tensile strength. When relying on physical models to describe structural behaviour under load, the material laws must first be accurately established. If the material laws either significantly over- or under-estimate the residual tensile capacity of the SFRC, an accurate physical model for the determination of its strength is not possible. However, in production control and materials specification, direct tensile testing is costly in time and difficult in that it requires specialised testing equipment. To this end, testing of prisms in bending is often substituted for uniaxial tension testing, and empirical design models are developed based on the results. Several attempts have been undertaken to provide an inverse analysis from prism data to establish the σ-w relationship but no direct test verification of the approaches have, to date, been established. This paper compares the results for σ-w relationship obtained from a direct tension test with those obtained using prism tests combined with an inverse analysis. Finally, a model is proposed that can be used for control testing with designs established using physically based models for strength limit states.

1 INTRODUCTION

Research into the use of steel fibres as reinforcement for shear and tensile actions in concrete members has been on-going for more than five decades [1-3] The tensile strength of plain concrete, being a quasi-brittle material, diminishes quickly to zero after cracking. For steel fibre reinforced concrete (SFRC), however, the fibres provide post-cracking tensile capacity due to the ability of the fibres to bridge and transmit tensile stresses across cracks. Depending on the mechanical and geometrical characteristics of the fibres, the presence of fibres can significantly improve the post-cracking tensile behaviour of the concrete.

One of the reasons for the limited utilisation of SFRC in structural applications has been the difficulty in establishing the characteristic tensile properties of the composite to a degree needed to be easily incorporated into existing or new design procedures. The most important property when considering the design of a structural member manufactured with SFRC is its post cracking, or residual, tensile strength.

Before cracking, the characteristic behaviour is generally represented by the tensile stress-strain response; after cracking, the behaviour is expressed in terms of stress versus crack opening displacement (σ-w)

relationship (Figure 1).

The σ-w relationship for SFRC can be directly obtained from a uniaxial tensile test, which is expensive in that it requires specialized equipment and is time consuming in its preparation, or indirectly after an inverse analysis from a three or four point bending test, as summarized in Figure 2.

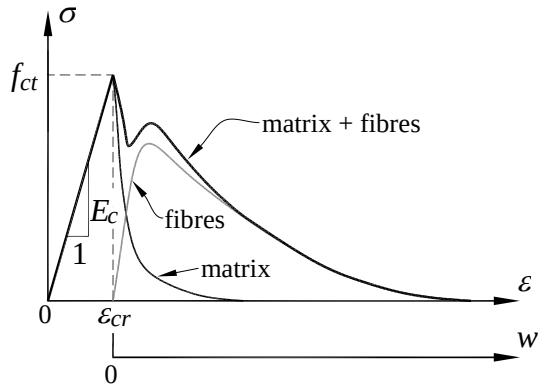

Figure 1: Stress versus strain/w for SFRC.

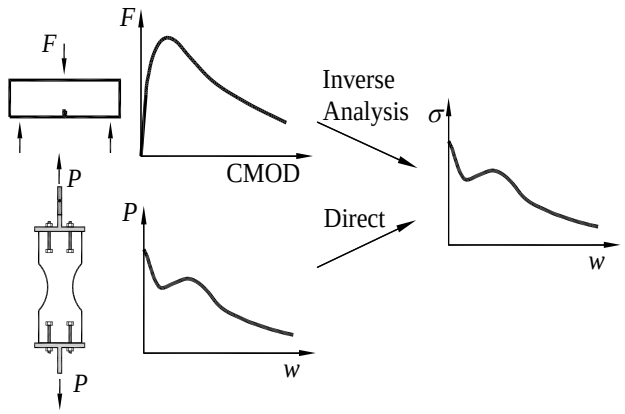

Figure 2: Approaches to determine the tensile properties of SFRC.

The use of three- or four-point bending tests on concrete prisms, together with an inverse analysis, to determine the tensile properties of SFRC has been described in [4]. The prism specimens may be notched or un-notched on the side of the extreme tensile fibre.

While a methodology for the determination of the tensile strength using prism tests has been established [5] and appears in the *fib* 2010 Model Code [6] using notched prism specimens, there is no data validating the approach against tension test data, rather validation has been sought from other means, such as FEM. While the *fib* prescribes a prism geometry, the methodology is independent of the specimen geometry or, indeed, on whether the prism is notched or un-notched or testing is by three- or four-point bending [5]. In this context, an experimental program is underway to investigate the tensile properties of several softening SFRC mixes. Some results of this project are reported in this paper.

2 EXPERIMENTAL INVESTIGATION

Four SFRC mixes (Table 1) were cast and tested. The SFRC mixes were fabricated using two types of commercially available steel fibres: end-hooked (EH) Dramix® RC-65/35-BN cold drawn wire fibres and OL13/0.20 straight (S) high carbon steel fibres; both manufactured by Bekaert. The EH fibres were 0.55 mm in diameter, 35 mm long and had a tensile strength of 1340 MPa. The S fibres were 0.2 mm in diameter, 13 mm long and had a tensile strength of more than 1800 MPa. The fibre volumetric dosages adopted in this study were 0.5% and 1.0% for both fibre types. The aggregate used was basalt with a maximum particle size of 10 mm.

The compressive strength characteristics of the concrete used in the study were determined from 100 mm diameter cylinders tested after 28 days of moist curing at 23^{o}C; the results are summarized in Table 1. The mean compressive strength (f_{cm}) was determined from three cylinders tested under load control at a rate of 20 MPa per minute, as per [7]. The modulus of elasticity (E_c) was obtained in accordance with [8]. The tensile strength of the matrix (f_{ct}) was obtained from the dog-bone tests (described below).

Table 1: Mechanical properties of SFRC mixes.

Mix	Fibre Type	Vol. (%)	f_{cm} (MPa)	E_c (GPa)	f_{ct} (MPa)
DA-0.5-EH	EH	0.5	56.2	33.0	3.85
DA-1.0-EH	EH	1.0	60.1	31.5	3.92
DA-0.5-S	S	0.5	63.7	34.7	4.03
DA-1.0-S	S	1.0	63.0	35.8	4.30

Note: EH = end-hooked; S = Straight.

The uniaxial tensile test was conducted on an hour glass shaped specimen, commonly referred to a "dogbone" specimen. This shape was introduced in [9]. Figure 3 shows the specimen size and test setup details adopted in this study.

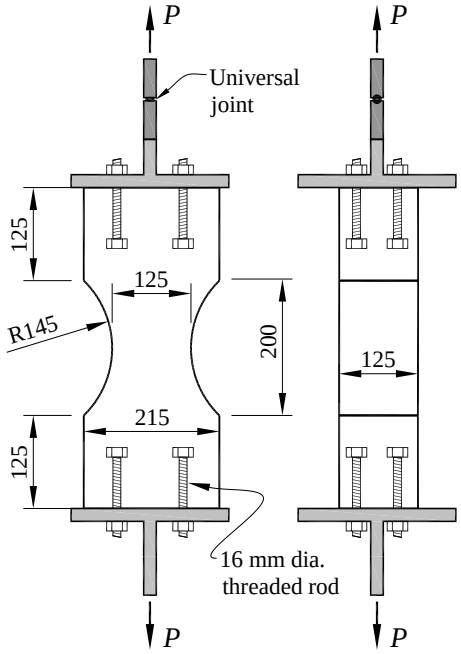

Figure 3: Details of uniaxial tension test specimens.

The dog-bone specimens were tested in an Instron servo-hydraulic testing machine. The specimens were connected to the testing machine via a series of bolted connections to 16 mm 8.8 grade threaded rods embedded 100 mm within the sample. One end of the test arrangement was connected to the testing machine through a universal joint, the other through a fixed platen.

To measure the crack opening displacement (COD), two LVDTs were attached to the North and South faces, with two LSCTs on the East and West faces of the specimen. The gauge lengths were 230 mm. The testing configuration and transducer arrangement is seen in Figure 4.

The load was applied using displacement control, initially at rate of 0.12 mm/min until the formation of the dominate crack. After cracking, the rate was increased to 0.2 mm/min with additional rate increases introduced as the test progressed.

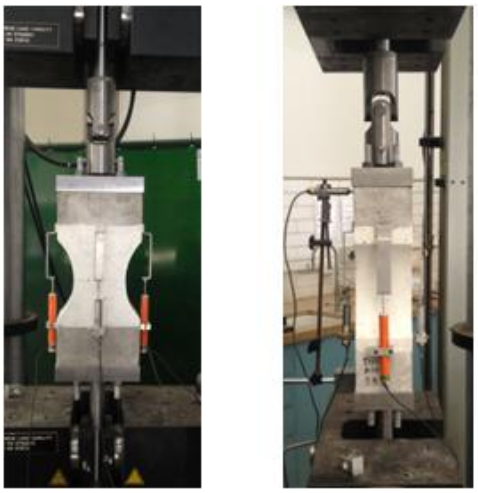

Figure 4: Photograph of uniaxial test showing transducers.

To establish the relationship for various specimen dimensions, and configurations, notched three-point beam tests were performed on two different sized prisms; 150 mm square section by 500 mm long prisms and 100 mm square section by 500 mm long prisms. The 150 mm square prisms had a notch depth of 45 mm; the 100 mm square prisms had a notch depth of 30 mm. The notches were cut with a diamond blade saw. The spans were 456 mm and 400 mm for the 150 mm and 100 mm square beams, respectively.

The prismatic specimens were tested using a closed loop test system by applying a clip gauge to the underside of the beam, at the notch, to measure and control the crack mouth opening displacement (CMOD) at the extreme tensile fibre. The test was operated such that the CMOD increased at a constant rate of 0.05 mm per minute, for the first two minutes, and then increased to 0.2 mm per minute until the CMOD reached 4 mm.

3 TEST RESULTS

The experimental results for the uniaxial tests are presented in Figures 5 to 8. Each curve represents the average of the four displacement transducers placed on the sides of the specimens. The points plotted on the axes of the figures are the tensile strengths of the matrix, with the averages for each series given in Table 1. In the figures plotting the uniaxial test results, no data is plotted between

the point of cracking and the stabilisation of the test immediately after cracking. This jump is due to the release of the elastic energy stored in the specimen, and is discussed below.

The load versus CMOD responses from the three-point notched bending tests are presented in Figures 9 to 12. Plotted within each of the figures are results from the two sized specimens (100 mm x 100 mm and 150 mm x 150 mm). The larger, 150 mm x 150 mm, prisms carry the higher loads.

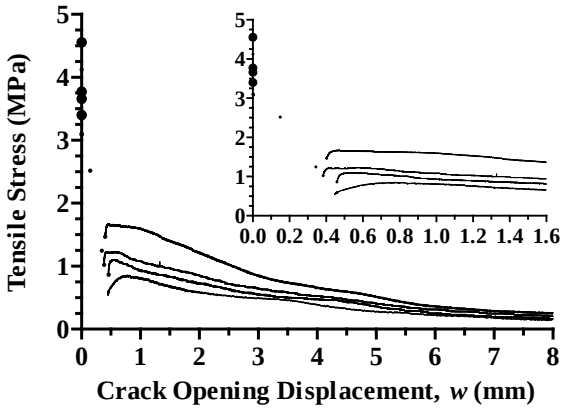

Figure 5: Uniaxial response of Mix DA-0.5-EH.

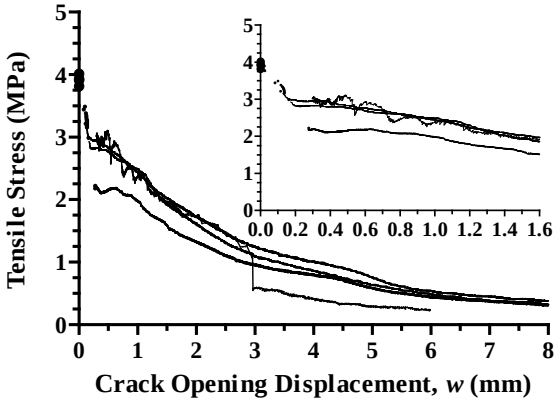

Figure 6: Uniaxial response of Mix DA-1.0-EH.

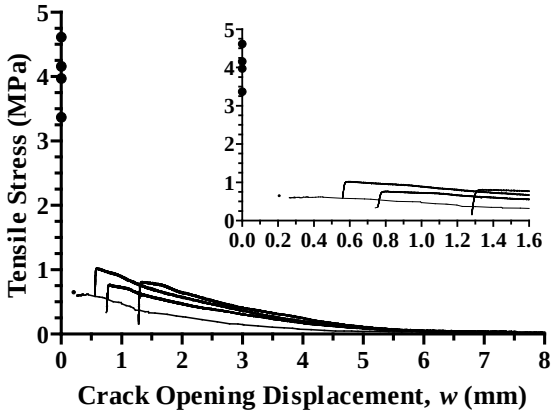

Figure 7: Uniaxial response of Mix DA-0.5-S.

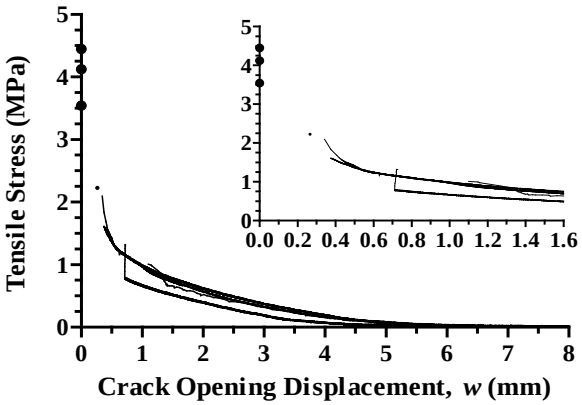

Figure 8: Uniaxial response of Mix DA-1.0-S.

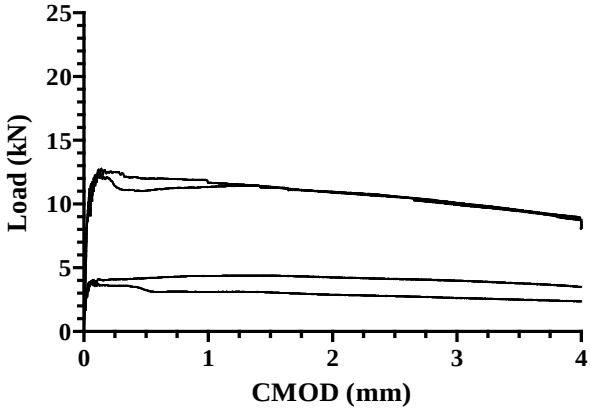

Figure 9: Flexural tensile strength for mix DA-0.5-EH.

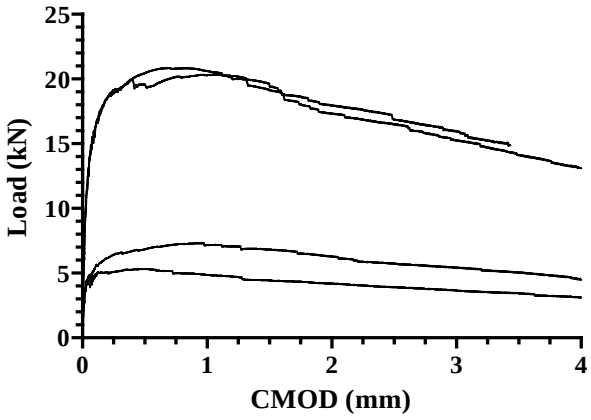

Figure 10: Flexural tensile strength for mix DA-1.0-EH.

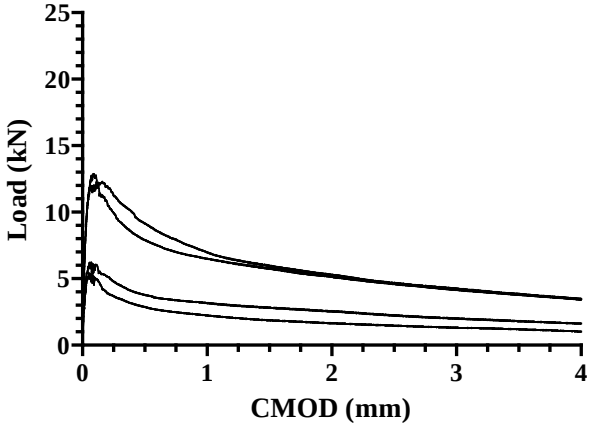

Figure 11: Flexural tensile strength for mix DA-0.5-S.

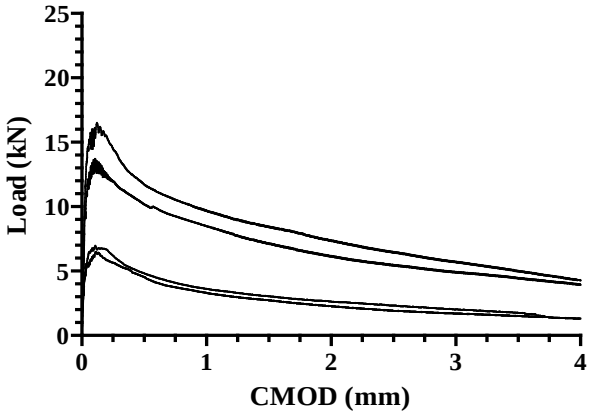

Figure 12: Flexural tensile strength for mix DA-1.0-S.

The fracture processes of all the direct tension specimens consisted of three key stages. The first stage involved the formation of a hairline crack of less than 0.05 mm width; once initiated, the crack propagated along the weakest cross section along a surface. At this stage, the peak stress had been achieved. This was shortly followed by a sharp reduction in load, coinciding with a significant opening of the crack, as the elastic strain energy stored in the specimen and testing rig was recovered. The degree of this initial step depended on the fibre type and quantity; once the crack is stabilised, the post-cracking residual strength beyond this point readily obtained. However, no displacement data is available between the peak load and that corresponding to the stabilised crack. After the crack had stabilised, the load again increased as the fibres became engaged. The long tail of the curves reflects the progressively smooth residual capacity of the specimens. Shortly after cracking it was clear that the concrete provided no contribution to the tensile strength and that the strength was due to the fibres alone.

Three distinct phases describe the response of the three-point notched bending test: (i) an elastic phase up to cracking; (ii) a flexural hardening response up to the onset of crack localization; (iii) a reduction of load with increasing CMOD.

The presence of a boundary restricts a fibre from being freely orientated [3,10]. An orientation factor, k_t, may be applied to the uniaxial test results to remove this influence, thus converting the results to that of an equivalent 3D fibre distribution free of boundary factors. For an element approximately square in section and tested in tension, as is the case in this study, the boundary influence found in [10] can be approximated as:

$$k_t = 0.5 \leq \frac{1}{0.94 + 0.6\, l_f / b} \leq 1 \qquad (1)$$

4 INVERSE ANALYSIS PROCEDURE

In this section, the inverse analysis procedure of the *fib* 2010 Model Code [6] is examined and a modified procedure proposed. By adopting an inverse analysis it is the intention to reproduce the tensile σ-w relationship from prism tests. Ideally, such a procedure should not depend on the test arrangement of the prism test, three- or four-point bending, span, notched or unnotched. Indeed the model of [5, 6] is generic in its formulation for the case of notched prism tests.

Figure 13(a) shows the cross-section for a SFRC prism cracked in bending where D is the total depth of the prism, h_{sp} is the depth minus the notch depth, d_n is the depth from the extreme compressive fibre to the neutral axis and b is the width of the prism. On the compressive side (Figure 13b), the strain at the extreme fibre is small relative to the strain to induce crushing of the concrete and the stress block may be considered as triangular. The stress at the extreme compressive fibre is σ_o.

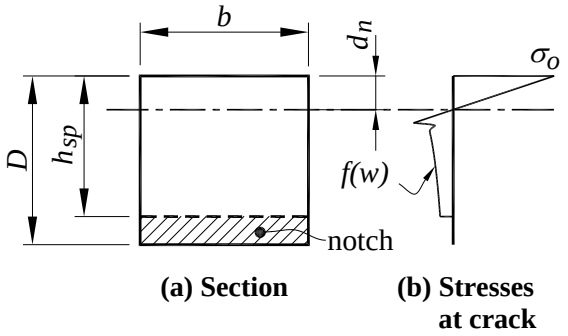

Figure 13: Model for inverse analysis of σ-*w* curve from prism bending tests

For a small length on the tensile side of the neutral axis (Figure 13b), the concrete is uncracked and carries tension. At greater

distances from the neutral axis, the concrete is cracked and the steel fibres carry a tensile stress *f(w)* that correspond to a direct tensile stress for a crack opening *w* at the level in the section under consideration.

Assuming that (i) at significant CMODs, the tensile component of the uncracked concrete can be ignored and (ii) rigid body rotations (Figure 14), the stress on the σ-w curve for the average COD between the root of the notch and the crack tip is denoted as f_w, and is calculated as:

$$f_w = \frac{2M}{h_{sp}^2\, b} = \frac{Fl}{2h_{sp}^2\, b} \qquad (2)$$

and is equivalent to that obtained by [5] using a rectangular stress block to describe internal tensile force provided by the fibres and with $d_n = 0$, and adopted in [6].

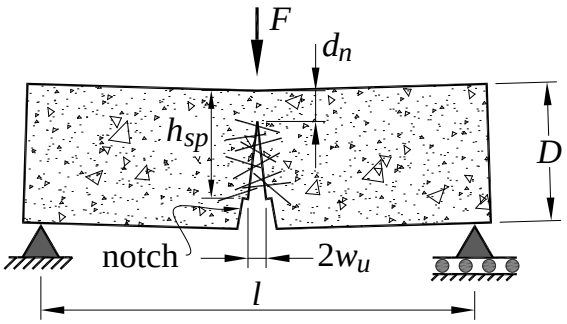

Figure 14: Determination of stress for an average width of w_u

Furthermore, assuming rigid body rotations of the two prism halves centred about the crack tip, the COD (w) for our σ-w curve is obtained from the measured CMOD as:

$$w = \frac{CMOD}{2} \cdot \frac{(h_{sp} - d_n)}{(D - d_n)} \qquad (3)$$

In Figure 15, the ratio of *w*/*CMOD* from Eq. 3 is plotted against the ratio d_n/h_{sp} for a 150 mm square prism with a 25 mm notch. The figure shows that at higher values of d_n, soon after cracking, *w* is about 0.38 times *CMOD*; at lower values of d_n, when the neutral axis is high in the section, *w* is 0.42 times *CMOD*, for this example. Thus, the results are somewhat insensitive to the neutral axis depth.

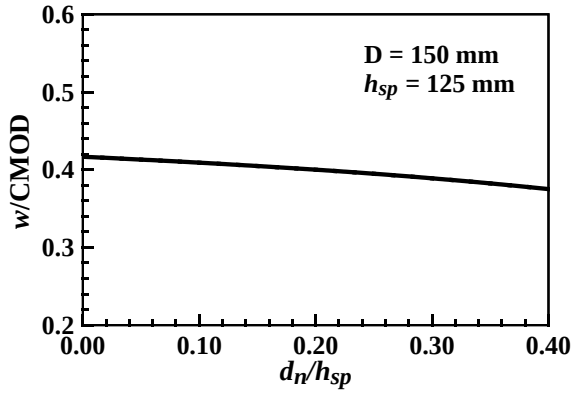

Figure 15: Ratio of *w*/CMOD versus d_n/h_{sp} for 150 mm square prism with a notch depth of 25 mm.

For design, an appropriately conservative value is recommended; taking $d_n = 0.3h_{sp}$ in Eq. 3 gives:

$$w = \frac{CMOD \times 0.35h_{sp}}{D - 0.3h_{sp}} \qquad (4)$$

In the establishment of Equations 2 to 4, it is assumed that sufficient cracking has occurred such that the neutral axis is sufficiently high in the section and, thus, the contribution of the uncracked concrete to the bending moment is small compared to that provided by the fibres. In determining a simple model, we adopt points corresponding to CMODs of 1.5 mm and 3.5 mm (which correspond to the points $CMOD_2$ and $CMOD_4$ according to [6]), which are sufficiently separated from each other to provide reasonable modelling over the most important region of the σ-w curve for both service and strength limit design and with the point $CMOD_2$ being sufficiently distant from initial cracking that the contribution of the uncracked concrete to the section capacity is of the prism is small.

Considering Equations 2-4 with a linear constitutive law, interpolating between points $CMOD_2$ and $CMOD_4$, gives:

$$f_w = \frac{f_{R2}}{3} + (f_{R4} - f_{R2})\, \xi(w) \geq 0 \qquad (5a)$$

$$\xi(w) = \frac{w}{3} \cdot \frac{(D - d_n)}{(h_{sp} - d_n)} - \frac{1}{4} \qquad (5b)$$

In Figures 16-19, the model of Equation 5 is compared to the direct tension test data compensated for the boundary effect by Equation 1. Also plotted is the prediction according to the equation of the *fib* 2010 Model Code [5, 6]. It is seen that the model given by Equation 5 developed in this paper correlates reasonably with the data up to $w \approx 1.5$ mm. Beyond $w = 1.5$ mm, the model becomes conservative. On the other hand, the Model Code relationship consistently over predicts the tensile strength for any given COD (w).

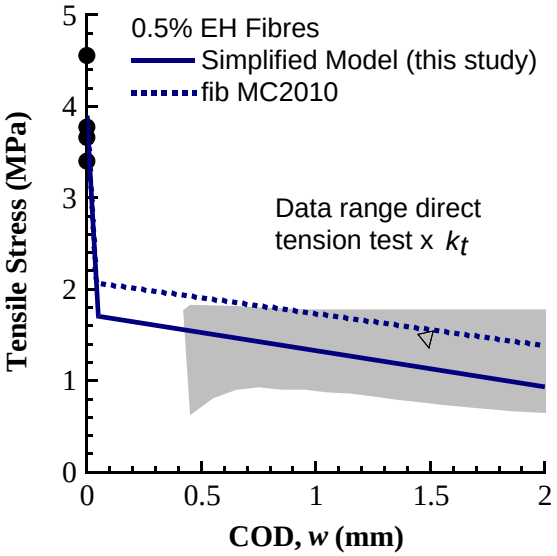

Figure 16: Comparison of proposed model with experimental data; Mix DA-0.5-EH

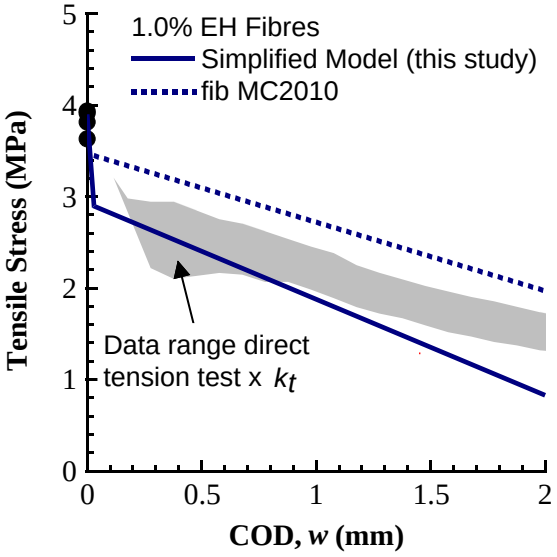

Figure 17: Comparison of proposed model with experimental data; Mix DA-1.0-EH

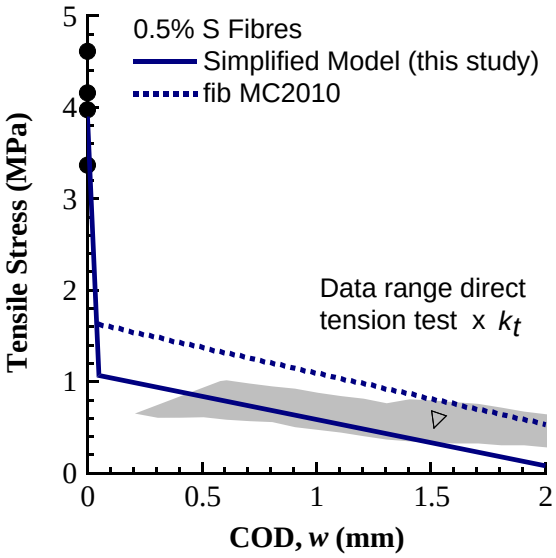

Figure 18: Comparison of proposed model with experimental data; Mix DA-0.5-S

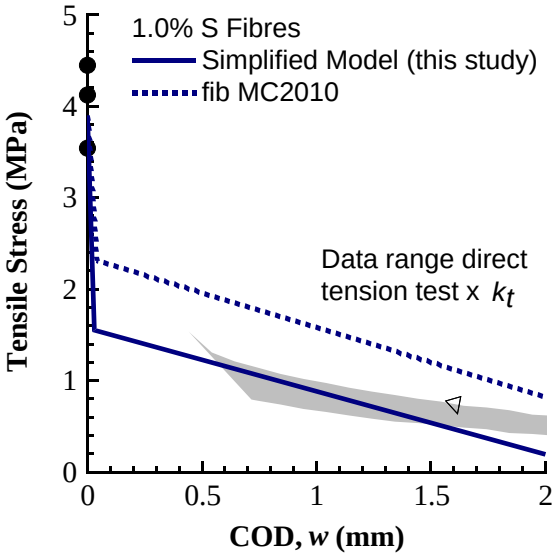

Figure 19: Comparison of proposed model with experimental data; Mix DA-1.0-S

The importance of the observation above should not be under stated. When relying on physical models to describe behaviour, such as for example shear, the material laws must first be accurately established. If the materials law either significantly over- or under-estimate the residual tensile capacity of the SFRC, an accurate physical model for the determination of strength is not possible and one is limited to empirical approaches to design.

5 CONCLUSIONS

In order to increase the utilization of SFRC in structural applications, it is important to correctly establish the post cracking or residual tensile strength of SFRC. The post cracking behaviour of SFRC can be obtained directly from uniaxial tensile tests, or indirectly following an inverse analysis of notched beams in bending. Consequently, reliable methods to attain these results are required.

Following an experimental investigation of four softening SFRC mixes and subsequent analysis that examined the applicability of developed inverse analysis techniques found in the literature, namely ones that led to the approach adopted in the *fib* 2010 Model Code [6], it was found that the Model Code results may significantly overestimate the residual tensile strength that form the basis of physical models for SFRC.

To address this, a simple, yet effective, inverse analysis procedure was derived to find the σ-w relationship for SFRC from prism bending tests. The model considers the influence of fibres on the moment carried by the specimen from the point in the test where the uncracked concrete has little influence of the capacity and considering rigid body rotations.

In the development of the model, it is important to note that the measurement point for the CMOD is not at the notch root (i.e. the location of the true crack mouth) but at a distance from it. With this observation a rational model is derived that is independent of specimen geometry, testing span and the method of testing, i.e. three- or four-point bending.

The model was validated against experimental data obtained from direct tension tests for four SFRC mixes. For all four mixes tested (two with end hooked fibres and two with straight fibres) and for two different prism sizes tested (100 mm square and 150 mm square), the model predicted the results well within the scatter range of the collected data.

REFERENCES

[1] Romualdi, J.P., & Batson. G.B. 1963. Behaviour of reinforced concrete beams with closely spaced reinforcement. *Proc., ACI J.* **60**(6): 775-789.

[2] Voo, J.Y.L. & Foster, S.J. 2004. Tensile fracture of fibre reinforced concrete: variable engagement model. In di Prisco, M., Felicett, R. & Plizzari, G.A. (eds.), *6th Rilem Symposium on Fibre Reinforced Concrete (FRC), Varenna, Italy, 20-22 Sept:* 875-884.

[3] Ng, T.S., Htut, T.N.S., & Foster, S.J. 2012. Fracture of steel fibre reinforced concrete - the unified variable engagement model. *UNICIV Report R-460*. School of Civil and Environmental Engineering, The University of New South Wales, Australia: 114 pp.

[4] de Oliveira e Sousa, J.L.A., Gettu, R. & Barragán B.E. 2002. Inverse analysis of the notched beam response for determining the σ-w curve for plain and fiber reinforced concretes. *Anales de Mecánica de la Fractura* **19**: 393-398.

[5] di Prisco, M., Plizzari, G. & Vandewalle, L. 2009. Fibre reinforced concrete: new design perspectives. *Mater and Struc* **42**:1261-1281.

[6] *fib* Model Code. 2010. *Model Code 2010-Final Draft, Vol.1, Bulletin 65*. Fédération Internationale du Béton: 350 pp.

[7] AS1012.9. 1999. Methods of Testing Concrete- Determination of the compressive strength of concrete specimens. Standards Australia.

[8] AS1012.17. 1997. Methods of Testing Concrete- Determination of the static chord modulus of elasticity and Poisson's ratio of concrete specimens. Standards Australia.

[9] van Vliet, M.R.A. 2000. Size effect in tensile fracture of concrete and rock. PhD thesis, Delft University, The Netherlands.

[10] Lee, S.C., Cho, J. & Vecchio, F. J., 2011. Diverse embedment model for steel fibre reinforced concrete in tension: model development. *ACI Mater J* **108**(5):516-525.